UV Raman Determination of the $\pi\pi^*$ Excited State Geometry of *N*-Methylacetamide: Vibrational Enhancement Pattern

X. G. Chen,[†] Sanford A. Asher,*[,†] Reinhard Schweitzer-Stenner,[‡,§] Noemi G. Mirkin,[‡] and Samuel Krimm[‡]

Contribution from the Department of Chemistry, University of Pittsburgh, Pittsburgh, Pennsylvania 15260, and the Biophysics Research Division, University of Michigan, Ann Arbor, Michigan 48109

Received August 8, 1994[⊗]

Abstract: We have examined the near-IR, visible, and UV Raman spectra of *N*-methylacetamide (NMA) isotopomers and characterized their Raman excitation profiles. We use the normal mode eigenvectors for these isotopomers to calculate a set of excited state bond displacements which are able to model the observed spectra of all of the isotopomers in water. The $\pi\pi^*$ excited state geometry for NMA in water differs from that of the ground state in that the CN bond elongates, while the CC and the N−CH_3 bonds contract by smaller amounts. The CO bond elongates by about 33% of that of the CN bond. Our results indicate that the alterations in the resonance Raman enhancement for NMA in non-hydrogen-bonding solvents involve both ground state normal mode composition changes and changes in the excited state geometry relative to the ground state. The CO bond becomes more elongated in the $\pi\pi^*$ excited state in the non-hydrogen-bonded solvents. The changes in the resonance Raman intensity in gas phase NMA result from an even larger NMA $\pi\pi^*$ excited state geometry expansion along the CO bond relative to the ground state. The C−CH_3 symmetric bending mode is enhanced, not due to its CH bending motion but because of the contribution of other internal coordinates.

Introduction

The continuing intense interest in the structure and dynamics of trans *N*-methylacetamide (NMA) derives, in part, because it is the simplest model for the amide linkage of peptides and proteins.[1-9] These studies are driven by the expectation that a clear understanding of the NMA ground and excited state structures and their potential energy landscapes is the basis for understanding the geometric constraints imposed by the peptide linkages that determine, in part, protein structure. Further, a detailed understanding of NMA spectroscopy is the fundamental basis for spectroscopic methods to monitor protein structure and dynamics.

The NMA ground state has planar symmetry in aqueous solution; however, a number of methyl rotational conformers with similar energies exist.[5,6] The excited state geometry of the NMA excited states is less clear, and recent UV Raman measurements have demonstrated facile monophotonic photoisomerization to the cis isomer of the ground state upon excitation within the amide $\pi \rightarrow \pi^*$ transition;[1c] this could indicate a twisted excited state geometry. Indeed, recent *ab initio* theoretical excited states calculations find twisted excited states for isolated NMA.[4a] The relevance of these calculational results to aqueous NMA is unclear since UV resonance Raman studies show dramatically different vibrational enhancement patterns for gas phase NMA, neat NMA, NMA dissolved in dry solvents, and NMA in aqueous solution.[1-3] This could result from different NMA excited state geometries and provide evidence for a strong dependence of the amide excited state geometry on the environment.

Numerous recent NMA UV resonance Raman studies have characterized the resonance Raman enhancement patterns.[1-3] In addition, recent normal mode calculations have utilized force constants determined from *ab initio* calculations of NMA hydrogen bonded to water molecules, which give a more reliable picture of the normal modes of NMA in water.[1d,6,7] For example, we recently demonstrated[8] that the NMA vibrational modes are significantly influenced by hydrogen bonding to water. The largest effect observed involves the amide I vibration, which is dominated by carbonyl stretching; the water bending motion is nearly degenerate with the amide I vibration, such that these motions couple, resulting in a dynamical entity that is the NMA−water cluster.

We recently reexamined the vibrational spectra of neat NMA and NMA in water and have spectrally resolved and assigned the bands observed with IR absorption spectroscopy, with polarized and depolarized nonresonance Raman spectroscopy and with UV resonance Raman spectroscopy.[1c,9] The results are surprisingly complex; the presence of cis and methyl group conformers and Fermi resonance interactions complicate the spectral assignments. We utilize these new assignments in the analysis here.

[†] University of Pittsburgh.
[‡] University of Michigan.
[§] Permanent Address: University of Bremen, FBI-Institute of Experimental Physics, 28359 Bremen, Germany.

[⊗] Abstract published in *Advance ACS Abstracts*, February 1, 1995.

(1) (a) Dudik, J. M.; Johnson, C. R.; Asher, S. A. *J. Phys. Chem.* **1985**, *89*, 3805−3814. (b) Krimm, S.; Song, S.; Asher, S. A. *J. Am. Chem. Soc.* **1989**, *111*, 4290−4294. (c) Song, S.; Asher, S. A.; Krimm, S.; Shaw, K. D. *J. Am. Chem. Soc.* **1991**, *113*, 1155−1163. (d) Mirkin, N. G.; Krimm, S. *J. Am. Chem. Soc.* **1991**, *113*, 9742−9747.

(2) (a) Mayne, L. C.; Ziegler, L. D.; Hudson, B. *J. Phys. Chem.* **1985**, *89*, 3395−3398. (b) Hudson, B. S. *Proc. SPIE-Int. Soc. Opt. Eng.* **1991**, *1403*, 27. (c) Harhay, G. P.; Hudson, B. S. *J. Phys. Chem.* **1993**, *97*, 8158−8164. (d) Hudson, B. S., Proceedings of the LALS conference, in press. (e) Mayne, L. C.; Hudson, B. *J. Phys. Chem.* **1991**, *95*, 2962−2967.

(3) (a) Wang, Y.; Purrello, R.; Jordan, T.; Spiro, T. G. *J. Am. Chem. Soc.* **1991**, *113*, 6359−6367. (b) Wang, Y.; Purrello, R.; Geogious, S.; Spiro, T. G. *J. Am. Chem. Soc.* **1991**, *113*, 6368−6377.

(4) (a) Li, Y.; Garrell, R. L.; Houk, K. N. *J. Am. Chem. Soc.* **1991**, *113*, 5895−5896. (b) Nitzsche, L. E.; Davidson, E. R. *J. Am. Chem. Soc.* **1978**, *100*, 7201−7204. (c) Triggs, N, E.; Valentini, J. J. *J. Phys. Chem.* **1992**, *6922*−6931. (d) Sugawara, Y.; Hirakawa, A. Y.; Tsuboi, M. *J. Mol. Spectrosc.* **1984**, *108*, 206. (e) Harada, I.; Takeuchi, H. *Spectroscopy of Biological Systems*; Clark, R. J. H., Hester, R. E., Eds.; John Wiley & Sons Ltd.: 1986; Vol. 13, pp 113−175.

(5) Gao, H.; Karplus, M. *J. Phys. Chem.* **1992**, *96*, 7273−7287.

(6) Mirkin, N. G.; Krimm, S. To be submitted.

(7) Williams, R. W. *Biopolymers* **1992**, *32*, 829−847.

(8) Chen, X. G.; Schweitzer-Stenner, R.; Mirkin, N. G.; Krimm, S.; Asher, S. A. *J. Am. Chem. Soc.* **1994**, *116*, 11141−11142.

(9) Chen, X. G.; Schweitzer-Stenner, R.; Asher, S. A.; Mirkin, N. G.; Krimm, S. *J. Phys. Chem.* In press (1995).

0002-7863/95/1517-2884$09.00/0

In this work we carefully examine the UV resonance Raman enhancement patterns of five isotopic derivatives of NMA whose normal compositions are well known.[1d] We analyse these data using the simplest set of assumptions to determine the distortions which occur for the NMA $\pi \rightarrow \pi^*$ excited state compared to the ground state. Our results indicate that the NMA $\pi \rightarrow \pi^*$ geometry changes differ between non-hydrogen-bonded NMA and NMA in water. This conclusion is consistent with recent calculational results of Hudson et al.[2d] The facile trans to cis $\pi \rightarrow \pi^*$ photoisomerization of NMA in water suggests a twisted excited state; however, the lack of enhancement of torsional overtones indicates a barrier to isomerization in the excited state manifold.

Experimental Section

Materials. *N*-Methylacetamide ($CH_3CONHCH_3$, NMA) was purchased from Aldrich Chemical Co. and distilled before use. *N*-Methylacetamide-d_3 ($CD_3CONHCH_3$, CD_3-NMA) and *N*-methylacetamide-$^{13}C_1$ ($^{13}CH_3CONHCH_3$) were synthesized by adding acetyl-d_3 chloride (Aldrich Chemical Co., 99% isotopic purity) or acetyl-$^{13}C_1$ chloride (Aldrich Chemical Co., 99% isotopic purity) to an excess of methylamine (Aldrich Chemical Co.) that was trapped at dry ice temperature. The purities of the final products were confirmed by proton NMR and mass spectra. D_2O (99.8%) was obtained from Cambridge Isotope Laboratories. NMA and CD_3-NMA were deuterated (ND) to form NMAD and CD_3-NMAD by dissolution in D_2O. Acetonitrile and ethylene glycol were obtained in the highest purity available from Baxter Diagnostics, Inc. The sample pH was adjusted by addition of aqueous solutions of 0.1 N HCl or NaOH. Sodium perchlorate (Aldrich Chemical Co.) was used as the internal intensity standard.

Instrumentation. Unless otherwise specified, the UVRR spectra were obtained by exciting samples flowing through a 1.0 mm i.d. Supracil quartz capillary. The Raman scattering measurements used a ca. 135° back scattering geometry. The Raman instrumentation is described in detail elsewhere.[10,11] We employed three different laser sources for the excitation profile studies. An intracavity frequency doubled CW Ar^+ laser source was used for 238 nm excitation[11a] The 217 nm laser excitation was generated by using a Nd:YAG laser system by mixing the doubled dye laser output with the 1064 nm Nd:YAG fundamental. The 210 nm excitation was obtained by doubling the output of a 100 Hz repetition rate excimer laser-pumped dye laser.[11c] The 192 and 200 nm excitations were obtained by stimulated Raman shifting of the second and fourth harmonics, respectively, of a Nd:YAG laser in hydrogen gas. The Raman shifter uses a 1 m stainless steel tube (1 in. i.d.) containing 30−70 psi of high-purity H_2. The output beam was separated from the fundamental and harmonics of the Nd:YAG laser by using two beam reflectors which have a high reflection efficiency (99%) for the unwanted incident beams. Two lenses ($f = 60$ cm) were used to focus the laser into the hydrogen shifter and to recollimate the Raman-shifted light. The desired UV excitation beam was selected by using a fused quartz Pellin−Brocca dispersing prism. The 200 nm and 192 excitation utilized pulse energies of 125 and 20 μJ at a 20 Hz repetition rate and were focused to ca. 250 μm diameter spot sizes at the sample.

The 1064 nm excited FT-Raman spectra were obtained by using a Nicolet 800 FT-IR spectrometer connected to an FT-Raman accessory. The samples were contained in stationary quartz capillaries. The absorption spectra were measured by using a Perkin-Elmer model Lambda 9 UV−vis−NIR spectrophotometer that was nitrogen purged for the shortest wavelength UV absorption measurements.

The peak values quoted were taken from the raw spectra, and we expect a precision of ±3 cm^{-1}. The deconvoluted peak frequencies are slightly different from the peak maxima indicated in the spectra due to spectral overlap.

Raman Cross Section Measurements. Raman cross sections were determined from the measured relative peak areas of the analyte to that of the $NaClO_4$ internal standard Raman band.[11d] These relative ratios were scaled by multiplication by our previously measured Raman cross sections of the internal standard 932 cm^{-1} band of $NaClO_4$ ($\lambda >$ 217 nm).[11d] The ClO_4^- Raman cross sections below 217 nm were calculated from the extrapolated values of the Albrecht-*A*-term expression[12] using the parameters determined by Dudik et al.[11d] This extrapolation should be reliable since the extrapolated resonance transition for ClO_4^- lies so deep in the UV.

The relative intensity ratios were corrected for both the instrument transfer function and self-adsorption. The instrument transfer function was determined for each excitation wavelength by using a calibrated standard D_2 lamp. When necessary, the areas of individual overlapping bands were deconvoluted by using the Galactic Industries Corp. Grams/386 software program. The self-absorption correction functions were obtained by measuring aqueous solutions containing $NaClO_4$ (0.5 M) and CH_3CN (1%) in the presence and absence of the absorbing NMA. We determined the self-absorption correction factors by determining the relative band intensities of the 381, 918, 1376, and 2249 cm^{-1} CH_3CN bands and the 932 cm^{-1} ClO_4^- band. The self-absorption correction function was significant for the deepest UV excitation, and its neglect could be responsible for the large differences between our calculated cross sections and those of Wang et al.;[3] they do not indicate that they corrected their data for self-absorption.

Results and Discussion

I. Normal Modes of NMA. Figure 1 compares the 1064 nm excited FT-Raman spectra of NMA, CD_3-NMA, NMAD, and CD_3-NMAD. Figure 2 shows UV Raman spectra of these isotopomers excited at different wavelengths. It is clear that only a small number of bands show large resonance enhancements.

The normal modes of NMA hydrogen bonded to two H_2O molecules, one at the carbonyl oxygen and the other at the amide hydrogen, were reported previously.[1d] In that calculation, *ab initio* force constants were calculated at the 4-31G* level and scaled by a least-squares optimization to the observed frequencies. We have extended those calculations to the isotopomers of interest in the present study, and the assignments of relevant bands are given in Table 1. One difference from the earlier results[1d,13] is that, in the present case, the CO out-of-plane bend (ob) scale factor, which is well determined by a secure assignment of the band at ~600 cm^{-1}, was separated from those of NH ob, NH···O ob, and CN torsion. This had the effect of predicting a more realistic value for the amide V mode. In addition, instead of keeping the bend scale factors for the two H_2O molecules the same,[1d] we adjusted the scale factor of the $(NH)H_2O$ to bring its frequencies in the range of those of the $(O)H_2O$; this is justified in view of the present artificial feature that the $(NH)H_2O$ does not participate in O−H···O hydrogen bonding, as does the $(O)H_2O$. In reality both do. The eigenvectors from these calculations were used in the analyses given below.

Although the assignments are discussed in detail elsewhere,[6,9] we wish to note some relevant features here. The nonenhanced bands of NMA include most of the out-of-plane modes[9] as well as in-plane modes at 1165 and 448 cm^{-1}, and their counterparts in the other isotopomers (see Table 1). The enhanced bands are the amide I, II, II′, and III modes for all of the isotopomers. For NMA, additional enhancement occurs for the ca. 1380 cm^{-1} CCH_3 symmetric bend (sb), for the 1418 cm^{-1} NCH_3 sb, and for the 883 and 632 cm^{-1} bands.

(10) (a) Asher, S. A. *Anal. Chem.* **1993**, *65*, 59A−66A. (b) Asher, S. A. *Anal. Chem.* **1993**, *65*, 201A−210A.

(11) (a) Asher, S. A.; Bormett, B. W.; Chen, X. G.; Lemmon, D. H.; Cho, N.; Peterson, P.; Arrigoni, M.; Spinelli, L.; Cannon, J. *Appl. Spectrosc.* **1993**, *47*, 628−633. (b) Asher, S. A.; Johnson, C. R.; Murtaugh, J. *Rev. Sci. Instr.* **1983**, *54*, 1657. (c) Jones, C. M.; DeVito, V. L.; Harmon, P. A.; S. A. *Appl. Spectr.* **1987**, *41*, 1268−1275. (d) Dudik, J. M.; Johnson, C. R.; Asher, S. A. *J. Chem. Phys.* **1985**, *82*, 1732−1740.

(12) Albrecht, A. C.; Hutley, M. C. J. *J. Chem. Phys.* **1971**, *55*, 4438.

(13) Mirkin, N. G.; Krimm, S. *J. Mol. Struct.* **1991**, *242*, 143−160.

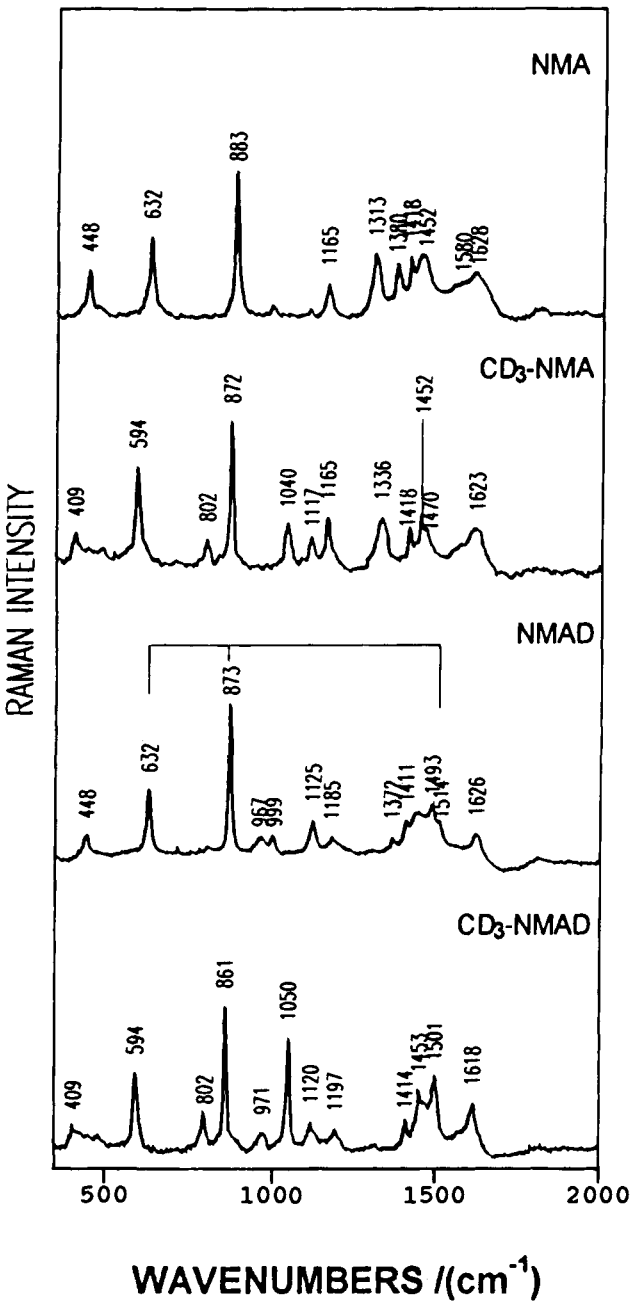

Figure 1. FT-Raman spectra excited at 1.06 mm of (A) 1.2 M *N*-methylacetamide (NMA) in H_2O, (B) 1.1 M CD_3-NMA in H_2O, (C) 1.3 M NMA in D_2O, and (D) 1.1 M CD_3-NMA in D_2O. The spectra were obtained with ca. 0.75 W laser power by accumulating 1000 scans over a period of 1000 s with 4 cm^{-1} resolution. The contribution from water has been numerically removed.

We recently demonstrated[8] that the UV Raman amide I band of NMA is complex, consisting of at least two components (of ca. 48 cm^{-1} half-width) at 1646 and 1626 cm^{-1}. The low-frequency band dominates with near-IR and visible excitation, while the high-frequency band dominates with excitation close to resonance in the UV. Normal mode analyses[8] showed that these components could result from coupling of CO stretch(es) with the bending mode(s) of the H_2O molecules(s) hydrogen bonded to the peptide group. (The present calculated splitting of 4 cm^{-1} between the components is to be compared with the 6 cm^{-1} splitting obtained with two H_2O molecules hydrogen bonded to the carbonyl oxygen.[7,8] This is less than the observed value of 20 cm^{-1}, but coupling of amide I with the actual water cluster hydrogen bonded to the peptide group could increase the predicted splitting.[8]) Although the amide I *relative* intensity is much smaller in the UV resonance Raman spectra (Figure 2) than in near-IR excited spectra (Figure 1), the *absolute* Raman cross section of the 1646 cm^{-1} component increases dramatically as excitation moves into resonance with the $\pi \rightarrow \pi^*$ transition at ca. 190 nm. While the potential energy distribution for this subband shows a smaller contribution of CNs compared to the dominant COs, the eigenvector displacement for CNs is only ~50% smaller than that for COs. We conclude that the CNs contribution, which is absent in the low-frequency component, is responsible for the selective enhancement of the 1646 cm^{-1} subband compared to that of the 1626 cm^{-1} subband. For NMAD and CD_3-NMAD, no such coupling of amide I to H_2O bend is possible (see Table 1), and their amide I bands are indeed singlets.

The amide II mode, at 1580 cm^{-1} in NMA, is barely observable with near-IR excitation (Figure 1) but dominates with UV resonance excitation (Figure 2). It consists mainly of CNs and NH in-plane bend (ib), obviously losing the latter component on N-deuteration. Upon deuteration of the nitrogen, the ND ib largely decouples from the CNs in the amide II′ bands of NMAD and CD_3-NMAD. Nevertheless, some ND ib remains in the enhanced amide II′ mode, even though the major ND ib mode is amide III′ at ca. 970 cm^{-1} in NMAD and CD_3-NMAD. The 1514, 1493 cm^{-1} doublet in NMAD derives from a Fermi resonance between amide II′ and the combination of the 872 and 632 cm^{-1} modes[6,9] (Figure 1). Although deconvolution of the amide II band indicates the presence of two subbands that probably derive from different methyl rotor conformations,[9] their relative intensities vary only slightly with wavelength, and we will ignore this complication in the work described here.

The amide III mode, at 1313 cm^{-1} in NMA, is strong with both near-IR and UV excitation. It also consists mainly of CNs and NH ib, but its CCH_3 sb component accounts for its shift to 1336 cm^{-1} on C-methyl deuteration.

The 1380 cm^{-1} band of NMA, which is intense with both near-IR excitation and UV resonance excitation, is mainly CCH_3 symmetric bend (sb) with a small CCs component. On N-deuteration, this mode becomes much weaker in the UV resonance Raman spectrum, and the CCs contribution to the normal mode drops significantly. The depolarization ratio of the 1380 cm^{-1} band is similar to that of amide III and is ca. 0.33 independent of excitation wavelength.[9] The depolarization ratio of the comparable band in NMAD is ca. 0.7, which indicates no strong enhancement by the amide $\pi \rightarrow \pi^*$ transition.[9] These results indicate, as discussed below, that the intensity of this band in NMA derives, both for visible and UV excitation, from preresonance with the amide $\pi \rightarrow \pi^*$ transition, and that pure CCH_3 sb is not Franck–Condon active in the excited state transition. Thus, we can conclude that the 1380 cm^{-1} band of NMA derives its enhancement through nuclear displacement coordinates other than CCH_3 sb.

The NCH_3 sb mode at 1418 cm^{-1} is observed with both UV and near-IR excitation. The 883 cm^{-1} skeletal deformation band, which is observed with both near IR and UV excitation, mainly consists of NCH_3 rock, CNs, CCs, and CNC deformation.

The amide IV bands of NMA and CD_3-NMA are observed in both the near-IR and UV Raman spectra at 632 and 594 cm^{-1}, respectively, while the amide IV′ bands of NMAD and CD_3-NMAD occur at 632 and 594 cm^{-1}, respectively. The amide IV and IV′ modes mainly involve NCO and CCO bending and CC stretching.

II. Excitation Profiles. Figure 2 compares the UV excited Raman spectra of the four isotopomers between 238 and 192 nm. Excitation of these compounds at 1064 nm (Figure 1)

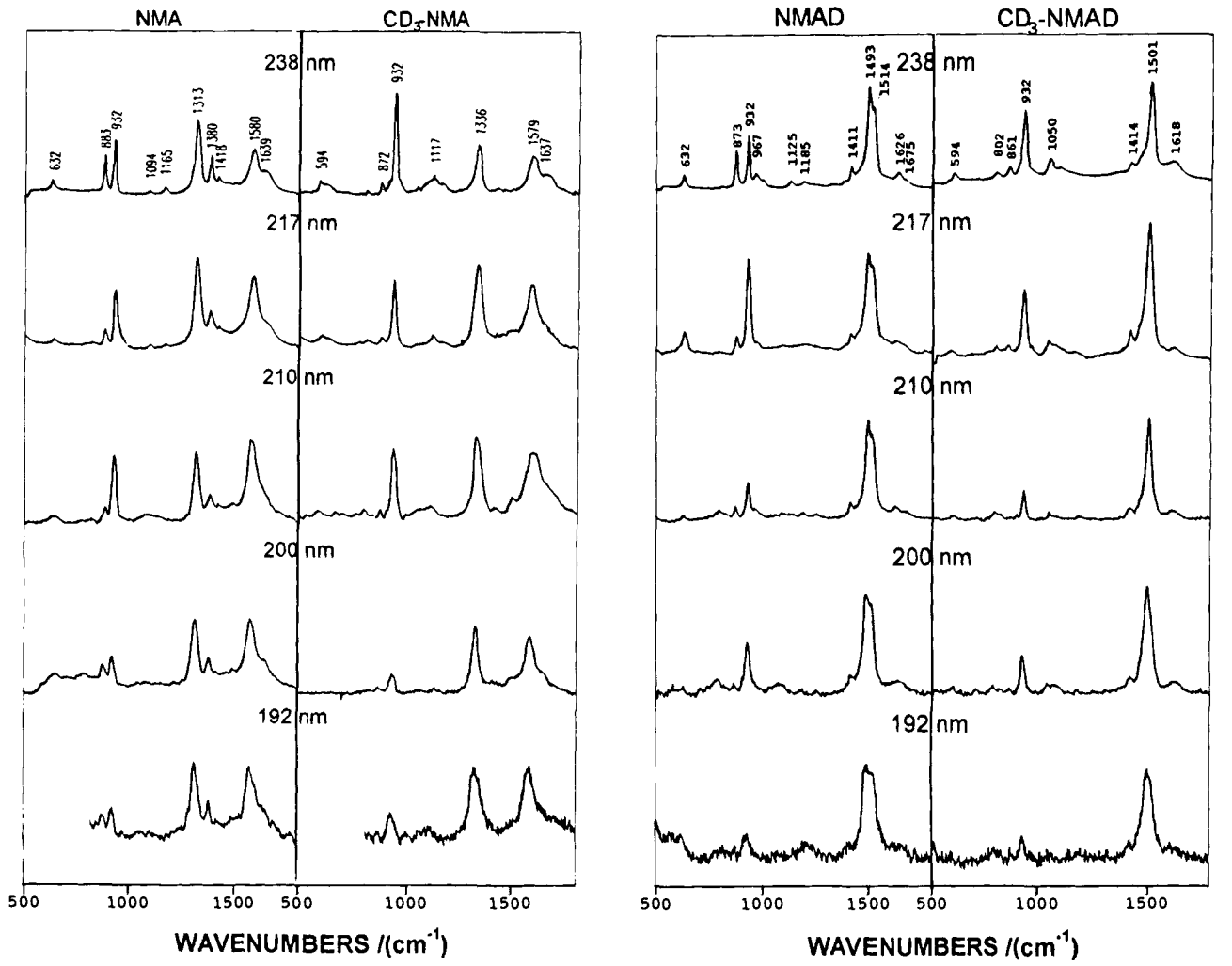

Figure 2. Raman spectra of NMA, CD_3-NMA, NMAD, and CD_3-NMAD as function of excitation wavelength. Sample concentrations are as follows. NMA: 194 mM at 238 nm, 49 mM at 217 nm, 9.8 mM at 210 nm, 3.6 mM at 200 nm, and 2.7 mM at 192 nm. CD_3-NMA; 196 mM at 238 nm, 50 mM at 217 nm, 9.9 mM at 210 nm, 4.2 mM at 200 nm, and 3.0 mM at 192 nm. NMAD: 111 mM at 238 nm, 23 mM at 217 nm, 8.4 mM at 210 nm, 3.0 mM at 200 nm, and 2.7 mM at 192 nm. CD_3-NMAD: 101 mM at 238 nm, 26 mM at 217 nm, 9.9 mM at 210 nm, 3.1 mM at 200 nm, and 2.6 mM at 192 nm. The 932 cm^{-1} band derives from ClO_4^- used as an internal standard. ClO_4^- concentration: 1.0 M for CD_3-NMA at 238 nm and NMAD at 217 nm; 0.3 M for NMAD at 238 nm; 0.5 M for the other spectra. Spectral resolution: ca. 5 cm^{-1} for 238 nm, 7 cm^{-1} for 217 nm, 12 cm^{-1} for 210, 14 cm^{-1} for 200 nm, 20 cm^{-1} for 192 nm spectra, respectively. The 238 nm excitation utilized 8 mW CW laser power, and the spectra were accumulated over a period of 6 min. The 217, 200 and 192 nm excited spectra were obtained at a 20 Hz repetition rate using 6 ns pulses with laser pulse energies of ca. 0.35, 0.10, and 0.020 mJ with accumulation times of 6, 20, and 35 min, respectively. The 210 nm spectra were obtained at a 100 Hz repetition rate using 16 ns pulses with laser pulse energies of 0.06 mJ with an accumulation time of 9 min.

occurs far from resonance, while 238 nm excitation approaches the preresonance condition. The Raman cross sections at selected excitation values are listed in Table 2. Excitation at 217 nm is well within the preresonance regime. Dudik et al.[1a] previously demonstrated that, even for excitation far from resonance, the amide II and III bands of NMA derive most of their intensity from preresonance enhancement from the amide $\pi \rightarrow \pi^*$ transition. From Dudik et al.'s[1a] data and our depolarization ratios,[9] we similarly expect that most of the intensity of the amide III band excited at 1064 nm results from the amide $\pi \rightarrow \pi^*$ transition. In contrast, excited far from resonance, the 632 and the 883 cm^{-1} bands derive most of their intensities from transitions deeper in the UV than the first amide $\pi \rightarrow \pi^*$ transition. As a result, the $\pi \rightarrow \pi^*$ transition dominates their intensities only when excitation occurs close to resonance. Little contribution is expected or observed from the weak NMA $n \rightarrow \pi^*$ transition.[1a]

Recently, Wang et al.[3a] reported that the amide I band is not significantly enhanced by the amide $\pi \rightarrow \pi^*$ transition at ca. 190 nm but is selectively enhanced by transitions further into the UV. Our data reported below contradict Wang et al.'s results;[3a] we find that in aqueous solution amide I is resonance enhanced by the amide $\pi \rightarrow \pi^*$ transition. Our new results as well as the theoretical analysis outlined below motivate us toward different conclusions concerning the amide $\pi\pi^*$ excited state geometry distortion.

The solid curves in the Figure 3 excitation profiles show preresonance Albrecht *A* term fits[12] to the Raman data for $\lambda >$ 211 nm. The calculated resonance transitions for NMA lie between 182 and 189 nm for all of the strong bands of all of the isotopomers (Table 3); these wavelengths are essentially identical to those of the amide $\pi \rightarrow \pi^*$ transition absorption maximum. Since the *A*-term expression is valid only in the preresonance regime, the excitation data at wavelengths below ca. 210 nm fall below the *A*-term curves. Our Raman cross section values are similar to those of Wang et al.[3a] in the preresonance regime but become 2-fold smaller in resonance. Probably this is the result of their failure to correct their data for self-absorption. The correct results would be smaller since the cross sections are determined from the ratios of intensities

Table 1. Observed and Calculated Frequencies (in cm^{-1}) of Some Modes of Hydrogen-Bonded NMA, CD_3-NMA, NMAD, and CD_3-NMAD

mode[a]	ν(obs)[b]	ν(calc)	potential energy distribution[c]
			NMA
		1632	CO s(39) (O)HOH b(35) (H)HOH b(11) CN s(10) CCN d(6)
Am I	1646		
		1631	(O)HOH b(54) CO s(19) (H)HOH b(16)
	1626	1628	(H)HOH b(86) CO s(17)
Am II	1580	1580	NH ib(45) CN s(41) CO ib(8) NC s(8) CO ib(8) CC s(7)
NCH_3 ab	1474	1469	NCH_3 ab(83) NCH_3 r(10) NCH_3 sb(6)
CCH_3 ab	1434	1444	CCH_3 ab(61) CCH_3 sb(17) NH ib(7)
NCH_3 sb	1416	1421	NCH_3 sb(93) NC s(5)
CCH_3 sb	1377	1381	CCH_3 sb(66) CCH_3 ab(24) CC s(8)
Am III	1313	1303	NH ib(30) CN s(18) CCH_3 sb(17) CO ib(11) CC s(6) CO s(5) NH-O b(5)
	1165	1173	NCH_3 r(50) NC s(13) CNC d(8) CO s(7) NCH_3 ab(6)
	1094	1097	NC s(52) CCH_3 r(12) CC s(9) NCH_3 r(9) CO ib(5)
Skel d	883	880	NCH_3 r(22) CN s(19) CC s(15) CNC d(9) CO ib(8) NC s(7) CCN d(6) CO s(6)
Am V		745	NH-O ob(41) CN t(38) NH ob(22) H-OH b(13) H-OH b(13)
Am IV	632	637	CO ib(35) CC s(34) CNC d(7) NC s(5)
	447	443	CCN d(52) CO ib(30) CCH_3 r(13) CNC d(8)
			CD_3-NMA
H_2O		1631	(O)HOH b(89)
H_2O		1629	(H)HOH b(103) CO s(6)
Am I	1619	1622	CO s(72) CCN d(11) CN s(10) (H)HOH b(9) NH ib(6)
Am II	1584	1578	CN s(45) NH ib(45) CO ib(8) NC s(8) CC s(5)
NCH_3 ab	1472	1468	NCH_3 ab(86) NCH_3 r(9) NCH_3 sb(6)
NCH_3 sb	1416	1421	NCH_3 sb(94) NCH_3 ab(6) NC s(6) CO s(5)
Am III	1334	1328	NH ib(37) CN s(19) CC s(19) CO ib(12) NH-O ib(6) NCH_3 sb(5)
	1165	1172	NCH_3 r(52) NC s(12) CNC d(9) CO s(6) NCH_3 ab(6)
CCD_3 sb	1117	1121	CCD_3 sb(39) NC s(31) CC s(21)
CCD_3 ab	1040	1042	CCD_3 ab(32) NC s(30) CCD_3 ab(21) NCH_3 r(7) CO ib(6)
Skel d	872	868	NCH_3 r(18) CC s(15) CO ib(12) CCD_3 sb(10) CNC d(9) CCN d(9) CO s(8) CN s(7)
	802	803	CCD_3 r(62) CN s(11) CO ib(7)
Am V		740	NH-O ob(44) CN t(38) NH ob(26)
Am IV	594	591	CC s(35) CO ib(24) NC s(5) CCD_3 r(5)
	409	408	CCN d(35) CO ib(29) CCD_3 r(20) CNC d(14) CO-H b(8)
			NMAD
Am I′	1626	1624	CO s(75) CN s(23) CCN d(10) CCH_3 r(5)
Am II′	1516	1518	CN s(41) CC s(19) CO ib(13) ND ib(12) NC s(9) CO s(7)
	1493	1505	873+632 combination (Fermi resonance)
NCH_3 ab	1476	1468	NCH_3 ab(87) NCH_3 r(10) NCH_3 sb(5)
CCH_3 ab	1436	1430	CCH_3 ab(70) NCH_3 sb(14) CCH_3 sb(6)
NCH_3 sb	1412	1415	NCH_3 sb(85) NC s(11) CCH_3 ab(8) CN s(5) NCH_3 ab(5)
CCH_3 sb	1371	1374	CCH_3 sb(88) CCH_3 ab(10)
	1185	1180	NCH_3 r(49) (O)DOD b(12) ND ib(6) CO ib(6) NCH_3 ab(6) CNC d(6)
	1125	1137	NC s(43) CCH_3 r(14) ND ib(11) CC s(9)
Am III′	967	950	ND ib(55) CCH_3 r(18) CN s(10) ND-O b(9)
Skel d	873	868	NCH_3 r(21) CN s(16) CC s(16) NC s(11) CNC d(8) CO ib(7) CCN d(6) ND ib(5)
Am IV′	632	634	CO ib(36) CC s(33) CNC d(7)
Am V′		529	ND-O ob(44) ND ob(36) CN t(33) D···OD b(13) D···OD b(13) CO ob(6)
	448	439	CCN d(52) CO ib(30) CCH_3 r(12) CNC d(9)
			CD_3-NMAD
Am I′	1616	1616	CO s(79) CN s(22) CCN d(11)
Am II′	1501	1510	CN s(48) CC s(17) CO ib(14) ND ib(14) NC s(10) CO s(6)
NCH_3 ab	1469	1468	NCH_3 ab(86) NCH_3 r(9) NCH_3 sb(6)
NCH_3 sb	1411	1416	NCH_3 sb(98) NC s(9)
	1197	1193	(D)DOD b(43) NCH_3 r(23) (O)DOD b(8) CC s(7) ND ib(6)
	1120	1146	NC s(37) CCD_3 sb(18) NCH_3 r(17) CC s(16) ND ib(5)
CCD_3 sb	1050	1050	CCD_3 sb(52) NC s(15) CCD_3 ab(7) ND ib(7) CN s(6) CO ib(5)
CCD_3 ab		1026	CCD_3 ab(89) CCD_3 sb(5)
Am III′	971	962	ND ib(47) NC s(22) ND-O ib(8)
Skel d	860	855	NCH_3 r(19) CC s(15) CO ib(11) ND ib(10) CCD_3 sb(9) CNC d(8) CCN d(8) CO s(6) CN s(6)
	802	798	CCD_3 r(61) CN s(12) CO ib(7)
Am IV′	594	588	CC s(34) CO ib(25) CNC d(5) CCD_3 r(5)
Am V′		516	ND ob(33) ND-O ob(31) CO ob(25) CCD_3 or(23) CN t(16)
	409	403	CCN d(38) CO ib(32) CCD_3 r(21) CNC d(15)

[a] Am, amide; ab, antisymmetric bend; sb, symmetric bend; skel, skeletal; d, deformation. [b] Based on spectrally deconvoluted bands (ref 9). [c] s, stretch; b, bend; ib, in-plane bend; ob, out-of-plane bend; r, rock; or, out-of-plane rock; t, torsion. (O)HOH: water molecule hydrogen bonded to carbonyl oxygen. (H)HOH: water molecule hydrogen bonded to amide hydrogen. Contributions ≥ 5. For definition of symmetry coordinates, see ref 1d.

of the high-frequency amide bands to the lower frequency internal standard band. In all cases, the internal standard band occurs at wavelengths with higher absorbances. An essential disagreement between our results and Wang et al.'s is that our data clearly show that the amide I′ band of NMAD in D_2O is enhanced by the amide $\pi \rightarrow \pi^*$ transition, while their data show no enhancement and indicate that the amide I′ enhancement derives from higher energy transitions. Their data appear to

Table 2. Raman Cross Sections of NMA, CD_3-NMA, NMAD, and CD_3-NMAD

	Raman cross sections (mbarn/mol·str)	
	200 nm	192 nm
	NMA	
1639 cm^{-1} (amide I)	125	192
1580 cm^{-1} (amide II)	507	750
1418 cm^{-1}	27.4	34.5
1380 cm^{-1}	132	183
1313 cm^{-1} (amide III)	459	772.5
883 cm^{-1}	40.3	142
632 cm^{-1} (amide IV)	35.2	94.8
	CD_3-NMA	
1637 cm^{-1} (amide I)	97.2	232
1579 cm^{-1} (amide II)	541	685
1420 cm^{-1}	29.5	5.64
1336 cm^{-1} (amide III)	565	739
872 cm^{-1}	34.5	124
594 cm^{-1} (amide IV)	30.5	117
	NMAD	
1626 cm^{-1} (amide I′)	132	181
1514/1493 cm^{-1} (amide II′)	1189	1624
1411 cm^{-1}	110.5	169
873 cm^{-1}	39.4	97.4
632 cm^{-1} (amide IV′)	36.2	136
	CD_3-NMAD	
1618 cm^{-1} (amide I′)	141	162
1501 cm^{-1} (amide II′)	862	1410
1414 cm^{-1}	96.8	279
1050 cm^{-1}	24.7	
861 cm^{-1}	31.9	72.6
594 cm^{-1} (amide IV′)	41.6	123

show that the excitation profile in resonance for the amide I′ band of NMAD in D_2O differs significantly from that of the amide II and III bands of NMA in H_2O. Our results clearly indicate that these excitation profiles are similar. We cannot explain these discrepancies.

In order to examine the enhancement of the strongly UV enhanced bands by the amide $\pi \rightarrow \pi^*$ transition, we examined the excitation wavelength dependence of the ratio of the intensities of these bands relative to those of the amide II and II′ bands (Figure 4); the amide II′ band is selectively enhanced by the amide $\pi \rightarrow \pi^*$ transition. A constant intensity ratio for a band relative to amide II′, as the excitation is varied *within* the $\pi \rightarrow \pi^*$ tansition, indicates that the band is enhanced by this transition. Thus, for NMA this type of analysis allows us to conclude that the 632, 883, 1380, and 1418 cm^{-1} bands and the amide I, II, and III bands are resonance enhanced by the amide $\pi \rightarrow \pi^*$ transition. For CD_3-NMA only the amide I, II, and III bands are resonance enhanced. For NMAD we conclude that the 873 and 1414 cm^{-1} bands and the amide I′ and II′ bands are resonance enhanced, while for CD_3-NMAD only the 1414 cm^{-1} band and the amide I′ and II′ bands are resonance enhanced by the amide $\pi \rightarrow \pi^*$ transition.

These constant amide I band relative intensities are not clearly evident from a cursory examination of the excitation profiles shown in Figure 3 since the amide I and I′ bands appear to show less curvature in their dispersion as resonance is approached. This occurs because the amide I and I′ bands show relatively large Raman cross sections at longer excitation wavelengths due to preresonance enhancement from transitions further in the UV. However, the amide $\pi \rightarrow \pi^*$ transition dominates the Raman cross sections with resonance excitation ($\lambda < 211$ nm). This is clearly evident in the Figure 4 plot of the relative ratio of the amide I′ to amide II′ bands of NMAD, where the ratio of 0.75, which occurs far from resonance, decreases to a constant value of 0.11 throughout the $\pi \rightarrow \pi^*$ transition resonance excitation data. The constant relative ratio of the Raman cross sections ($\lambda < 211$ nm) clearly indicates that the source of the amide I′ enhancement is the amide $\pi \rightarrow \pi^*$ transition at ca. 190 nm.

The dispersion of the depolarization ratio is a more sensitive, but more complex, indicator of the enhancement mechanism. The 0.33 value of the depolarization ratio of the amide III band and the 1380 cm^{-1} CCH_3 sb mode indicates dominating enhancement by the amide $\pi \rightarrow \pi^*$ transition, even with visible wavelength excitation. However, the amide II depolarization ratio of 0.12 at 514 nm and 0.28 in the UV below 244 nm indicates that, far from resonance, amide II gains intensity from other electronic transitions in addition to the amide $\pi \rightarrow \pi^*$ transition.[9]

III. Resonance Enhancement and the NMA Excited State Geometry. Resonance Raman excitation within strongly allowed electronic transitions enhances those vibrations that deform the ground state geometry toward that of the excited state. Numerous theoretical approaches exist to interpret the observd resonance Raman intensities in terms of molecular excited state geometries and potential function changes.[14-19] These approaches involve either approximations based on the Kramers–Heisenberg sum-over-states approach[12] or the time-dependent Raman theory formalism.[14a] In principle, it is possible to quantitatively determine the excited state geometry changes and excited state potential function changes for NMA because it is a relatively small molecule, and it appears that a single electronic transition is responsible for the Raman enhancements in the 230–185 nm spectral region. The solution to this problem should be greatly aided by the previously calculated ground state normal modes.[1d] However, impediments to this task result from the fact that we cannot as yet measure the entire absorption spectrum or the Raman excitation profiles on the high-energy side of the amide $\pi \rightarrow \pi^*$ transition; we are unable to measure spectra below 185 nm.

Some information on the π^* excited state of NMA may be obtained from the recent calculation by Li et al.[4a] that indicates that the relaxed form of the first and second amide $\pi\pi^*$ excited states are nonplanar and that the CN and CO bonds elongate and the C(O) and N pyramidilize. This calculation, however, also indicates that additional energy minima may occur on the excited state potential surface. However, the portion of the excited state surface probed by the Raman experiment may differ from the portion of the surface around the relaxed $\pi\pi^*$ equilibrium geometry; the Raman scattering generally most heavily weights that portion of the excited state surface situated around the ground state equilibrium geometry.[14a]

This may be especially relevant for NMA since it appears that the $\pi\pi^*$ excited state twists and permits a facile trans–cis photoisomerization.[1c] The fat that we do not observe enhancement of the amide group's torsional modes probably indicates that a barrier exists in the excited state surface between the

(14) (a) Myers, A. B.; Mathies, R. A. *Biological Applications of Raman Spectroscopy*; Spiro, T. G., Ed.; John Wiley & Sons Inc., 1987; Vol. 2, pp 1–58. (b) Chinsky, L.; Laigle, A.; Peticolas, W. L.; Turpin, P.-Y. *J. Chem. Phys.* **1982**, *76*, 1–4.

(15) Shin, K. K.-S.; Zink, J. I. *Inorg. Chem.* **1989**, *28*, 4358–4366.

(16) Reid, P. J.; Lawless, M. K.; Wickham, S. D.; Mathies, R. A. *J. Phys. Chem.* **1994**, *98*, 5597–5606.

(17) Wright, P. G.; Stein, P.; Burke, J. M.; Spiro, T. G. *J. Am. Chem. Soc.* **1979**, *101*, 3531–3535.

(18) (a) Peticolas, W. L.; Blazej, D. C. *Chem. Phys. Lett.* **1979**, *63*, 604. (b) Blazej, D. C.; Peticolas, W. L. *J. Chem. Phys.* **1980**, *72*, 3134–4142. (c) Peticolas, W. L.; Rush, J., III. In *Proceedings of the IV International Conference on Raman Spectroscopy*; Yu, N.-T.; Li, X.-Y., Eds.; John Wiley and Sons: New York, 1994; pp 39–42. (d) Peticolas, W. L. Personal communication.

(19) Warshel, A.; Dauber, P. L. *J. Chem. Phys.* **1977**, *66*, 5477.

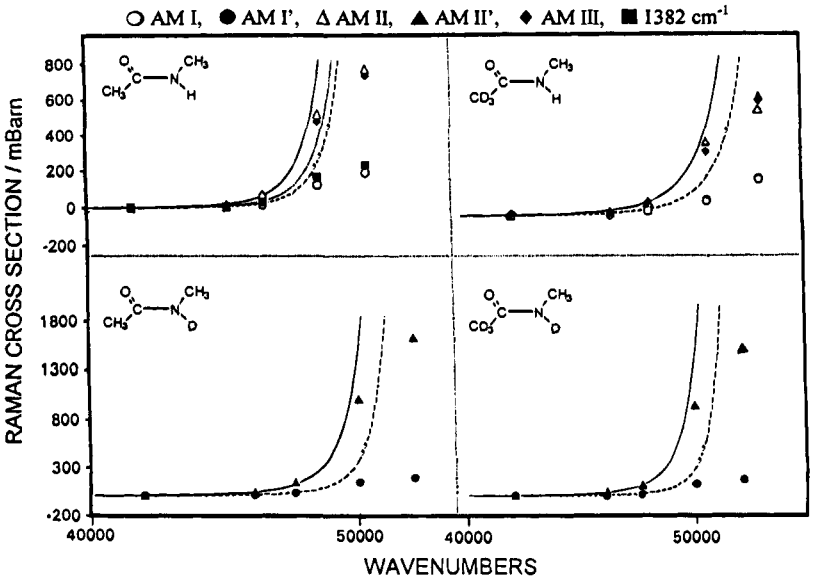

Figure 3. Resonance Raman excitation profiles of NMA, CD_3-NMA, NMAD, and CD_3-NMAD. Solid lines correspond to nonlinear least-squares best fits of preresonance data ($\lambda \geq 211$ nm) to the Albrecht A-term expression.[12]

Table 3. Albrecht A-Term[12] Fitting Parameters and Excited State Frequencies[a]

mode (cm^{-1})	$K \times 10^{-29}$	ν_e (nm)
	NMA	
Am I	3.51	186
Am II	6.01	188
Am III	4.55	183
1380	4.49	186
	CD_3-NMA	
Am I	1.7	183
Am II	2.3	186
Am III	1.05	182
	NMAD	
Am I	8.91	189
Am II	3.31	188
	CD_3-NMAD	
Am I	2.01	188
Am II	7.91	189

[a] A-term preresonance fitting utilized data excited at $\lambda > 211$ nm.

twisted minimum and the portion reached by a vertical transition from the planar trans ground state.[20] Thus, resonance Raman excitation of trans NMA may selectively probe the region of the excited state around the vertical transition.

Because of the present lack of certainty concerning the excited state potential function and the excited state structure, and because of our inability to measure the complete Raman excitation profiles and absorption spectrum, we are forced to model our resonance Raman data using the simplest theoretical approach that relates the observed Raman cross sections to displacements in the excited state geometries along the normal mode coordinates.[14-19] This theoretical approach derives from the sum-over-states Kramers–Heisenberg expression, in which only one electronic resonance transition is involved in the enhancement. This approach assumes that the ground and excited state normal modes and force constants are identical and that enhancement occurs due to A-term activity within a strongly allowed electric dipole transition.

We realize that some of these assumptions are not completely satisfied, but we expect that the errors associated with the failure of these assumptions cause quantitative rather than qualitative errors; an alteration of either a bond length or a force constant

(20) Ci, X.; Myers, A. B. *J. Chem. Phys.* **1992**, *96*, 6433–6442.

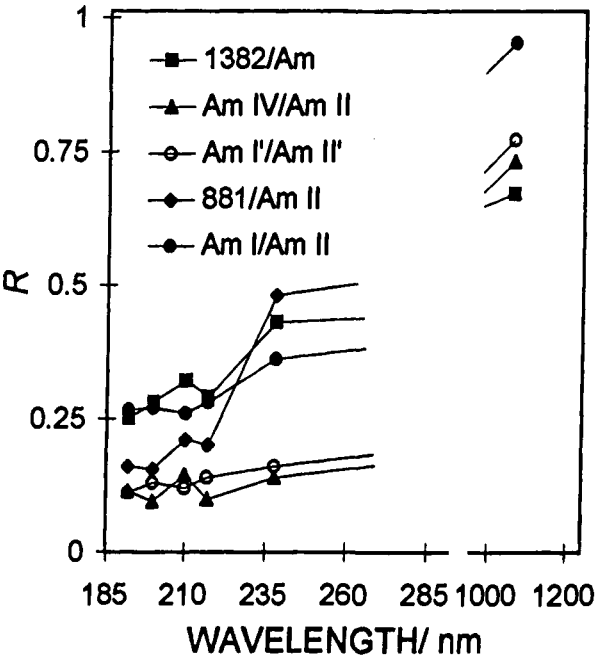

Figure 4. Excitation wavelength dependence of the relative intensity ratio of various NMA bands relative to the amide II band and of the NMAD bands relative to the amide II′ band.

will result In resonance Raman enhancement of those vibrations that involve that internal coordinate. In addition, it has recently been shown that the simple relationship between Raman intensities and excited state displacements (eq 1) is exact even for large displacements.[18c,d]

Equation 1 implicitly assumes the approximations above and relates the magnitudes of the Raman intensities of normal mode i I_i to the displacement of the excited state Δ_i (dimensionless coordinates) along the ith normal coordinate of frequency ω_i:

$$I_i \approx \frac{\Delta_i^2 \omega_i^2}{((\Delta\nu)^2 + \omega_i \Delta\nu - \Gamma^2)^2 + (2\Gamma\Delta\nu + \Gamma\omega_i)^2} \quad (1)$$

where $\Delta\nu$ is the frequency difference between the excitation frequency and the frequency of the 0–0 electronic transition.

Table 4. Relative Bond Length Changes of CD_3-NMA in Water

bond	relative bond length changes			
ΔCN	1	0.6	1	0.4
ΔCO	−0.2	−1	0.3	0
ΔCC	−0.6	0.7	−1	0.6
ΔNC	−0.4	−0.1	−0.6	−0.5
ΔNH	0	0.3	0	1
$\Delta C^{\alpha}H$	0	0	0	−0.1
$\Delta C^{\beta}H$	0	0.1	0	0.1
band/cm^{-1}	sign combinations			
amide I	+	+	−	−
amide II	+	+	+	+
amide III	+	−	+	−

Γ is the reciprocal of the homogeneous line width of the resonance transition, which we assume is independent of the vibronic transition. For excitation within resonance, $\Delta\nu = 0$ and the cross sections are directly proportional to the square of the displacements. For the case of NMA, for which a large homogeneous line width is likely,[2b,c] the Raman cross sections will also scale as the square of the vibrational frequency. Thus, low-frequency modes require a larger Δ_i than high-frequency modes to have comparable cross sections. For resonance excitation, the relative cross sections of the Raman bands are determined by the relative displacements Δ_i along each of the normal coordinates.

We can relate[14-19] the displacement along the normal coordinate to displacements of the atoms of NMA through eq 2:

$$\Delta r_j = \sum_i L_{ij} \frac{\Delta_i}{0.17\sqrt{m_j \omega_i}} \qquad (2)$$

where Δr_j is the Cartesian displacement (Å associated with atom j of mass m_j). L_{ij} are the matrix elements which transform the normal mode coordinates to Cartesian coordinates. These L_{ij} elements are determined in our normal mode calculations. From these expressions it is possible to estimate the *relative* geometry change that occurs during the vertical electronic transition to the $\pi\pi^*$ excited state. Unfortunately, the sign of Δ_i is indeterminate, and we can only determine the numerous possible relative displacements, each of which is associated with a particular sign of Δ_i.

For NMA, the situation is more constrained since we have four isotopomers for which we have determined the individual relative $|\Delta_i|$ for each of the normal modes. The electronic absorption spectra of these derivatives are identical. Therefore, the excited state geometries are similarly shifted compared to the ground states, and we must obtain identical relative excited state displacements for all four isotopomers; we include in our calculation only those bands that we were able to document were enhanced by the amide $\pi \rightarrow \pi^*$ transition.

For CD_3-NMA and CD_3-NMAD, the situation is relatively simple since only three modes have significant intensity (Tables 4 and 5). For CD_3-NMAD, all possible sign combinations show that little change occurs in the ND bond length. This fact allow us to eliminate from consideration columns 2 and 4 of the solutions for CD_3-NMA. The remaining solutions for CD_3-NMA both indicate that the smallest change occurs in the CO bond length. This fact can be used to discard column 2 for CD_3-NMAD and makes column 1 unlikely. The final two possibilities for CD_3-NMAD are very similar; the major bond length change occurs for the CN bond. We expect that this represents an elongation if the calculation of Li et al.[4a] and the results of others have any reliability for aqueous NMA. Thus, the CC bond and the NC bond contract by ca. 50% of the amount the CN bond expands. This allows us to select column 1 of CD_3-NMA as the correct solution since the CC bond contraction is too large in column 3. It appears that the NC bond may contract less than the CC bond.

For NMAD, four vibrations are enhanced and eight unique possibilities exist (Table 5). We can immediately discard columns 1−4, which yield a large CO bond length change. Column 5 is discarded because it gives too large an ND bond length change. Column 6 is unlikely since it suggests too large a CC bond contraction. The most likely solutions are given by either column 7 or 8, which only differ in their relative amounts of NC bond elongation.

The situation for NMA is very complex since the 7 enhanced vibrations result in 64 unique possibilities. We can find numerous solutions similar to those above within these 64 combinations. Indeed, if we only consider the four most intense bands (amide I, II, III, and the 1380 cm^{-1} band), we discover two solutions which fit the criteria discovered above, viz., columns 3 and 8 of Table 6. For these solutions, the CN bond length change is largest, while the CO bond length change is smallest, CC is intermediate and NC is smaller; the NH bond barely changes.

These results were used as the starting point to determine the best set of relative displacements along the internal coordinates that simultaneously predict all of the aqueous NMA isotopomer resonance Raman spectra (Table 7). We iterated

Table 5. Relative Bond Length Changes of CD_3-NMAD and NMAD in Water

bond	relative bond length change											
	CD_3-NMAD				NMAD							
ΔCN	1	0.8	1	1	1	0.9	0.5	0.9	1	1	1	1
ΔCO	0.7	0.9	0	0.1	0.8	0.8	0.7	1	−0.1	0	0.1	0.1
ΔCC	−1	−1	−0.5	−0.6	−0.9	−0.2	−1	−1	−0.8	−0.9	−0.5	−0.6
ΔNC	−0.8	−0.4	−0.5	−0.3	−0.6	−1	−0.4	−0.3	−0.7	−0.5	−0.5	−0.2
ΔND	0.1	0.1	0.1	0.1	0	0.1	0	0	0.7	0.1	0	0
$\Delta C^{\alpha}H$	0.1	0.1	0	0	0	0	0	0	0	0	0	0
$\Delta C^{\beta}H$	0.1	0	0	0	0	0.1	0	0	0	0.1	0	0
	sign combinations											
band/cm^{-1}	Signs				Signs							
amide I′	+	+	−	−	+	+	+	+	−	−	−	−
amide II′	+	+	+	+	+	+	+	+	+	+	+	+
1414	+	−	+	−	+	+	−	−	+	−	+	−
873					+	−	−	+	−	−	+	+

Table 6. Relative Bond Length Changes of NMA in Water

	relative bond length change							
ΔCN	1	0.62	1	0.80	0.68	0.36	1	1
ΔCO	−0.11	−1	−0.15	−1	0.01	0.38	0.54	0.40
ΔCC	−0.29	0.57	−0.55	−0.13	−1	0.34	−0.64	−0.91
ΔNC	−0.41	−0.08	−0.42	−0.20	−0.60	−0.61	−0.61	−0.60
ΔNH	−0.02	0.24	0.02	0.14	0.43	1	0.01	0
$\Delta C^{\alpha}H$	0	−0.04	0.03	0.10	0.19	−0.16	0.01	0.04
$\Delta C^{\beta}H$	0	0.1	0.06	0.04	0.08	0.19	0	0.07
band/cm^{-1}	sign combinations							
amide I	+	+	+	+	−	−	−	−
amide II	+	+	+	+	+	+	+	+
1380	+	+	−	−	−	+	+	−
amide III	+	−	+	−	−	−	+	+

Table 7. Relative Excited State Displacements of NMA and Its Isotopomers in Water, in CH_3CN, and in the Gas Phase

displacements	H_2O	CH_3CN	gas phase
ΔCN	1	1	1
ΔCO	0.29	0.41	0.76
ΔCC	−0.66	−0.52	−0.41
ΔNC	−0.4	−0.33	−0.20
ΔNH	0	0	0
$\Delta C^{\alpha}H$	0	0	0
$\Delta C^{\beta}H$	0	0	0

the displacements along only the CN, CO, CC, and NC bonds since the results above show negligible values for other displacements. The best-fit displacements were determined by variation of the displacements with visual inspection to determine which set of displacements resulted in calculated spectra that best modeled the measured spectra simultaneously for all of the isotopomers. As expected from the results for the individual isotopomers, the largest bond length change is an expansion along the CN bond, which is accompanied by smaller contractions along the CC and NC bonds. The best fit displacements indicate that an expansion also occurs along the CO bond. This displacement should have the largest uncertainty. This increased uncertainty results from the weak intensities of the amide I band in the measured spectra, the complications of the amide I band normal mode distribution, and the approximations involved in our theoretical treatment.

These best-fit displacements are used to calculate the resonance Raman spectra shown in Figure 5; these spectra closely resemble the 200 and 192 nm isotopomer experimental spectra shown in Figure 2. These calculated spectra assumed Gaussian band shapes and bandwidths similar to those we determined recently for the isotopomers.[9] The band frequencies were those experimentally determined. For the amide I and amide II bands, we neglected the complications of the overlapping subbands and used 45 cm^{-1} bandwidths.[8]

There is excellent agreement in the relative intensities of the calculated spectra compared to the experimental spectra. Table 7 displays the best-fit displacements, while Table 8 displays the relative intensities and the Raman cross sections of the different isotopomers. The relative Raman cross sections can be compared between isotopomers. For NMA we correctly predict that only the amide II and III and the 1380 cm^{-1} bands are strongly enhanced. For CD_3-NMA, we correctly predict that the CCD_3 sb band disappears and for NMAD and CD_3-NMAD that the amide II′ band dominates the spectra. We predict that the amide II′ intensities are ca. 3-fold larger than that of the amide II band; we measure a smaller increase of 2.2

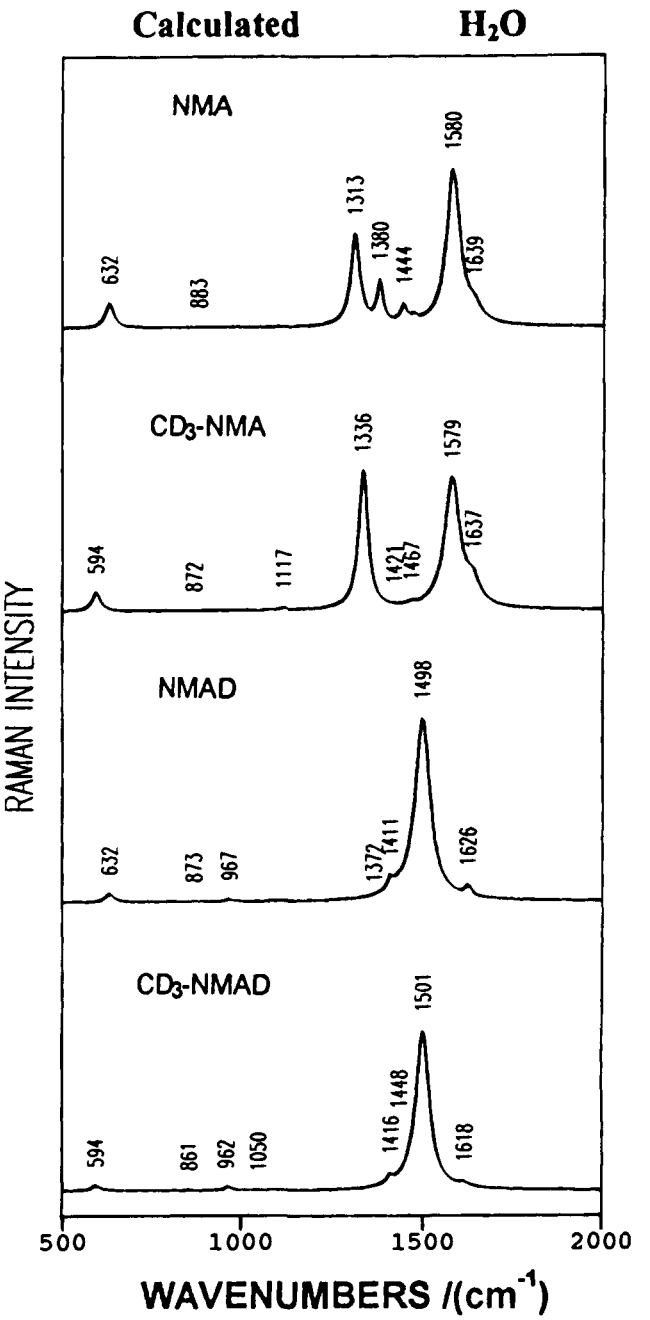

Figure 5. Calculated 200 nm excited resonance Raman spectra of aqueous trans NMA, NMAD, CD_3-NMA, and CD_3-NMAD in H_2O. The spectra were calculated using the measured frequencies of the bands, a 45 cm^{-1} bandwidth for the amide I and II bands, a 30 cm^{-1} bandwidth for the amide III and IV bands, and 20 cm^{-1} for the other bands.

(Table 2). We correctly predict the relative weaknesses of the amide I and I′ bands and predict small or negligible intensity for the other vibrations of the NMA isotopomers.

The best-fit displacements for NMA isotopomers in water indicate that the CN bond undergoes the largest displacement, which is expected to be an expansion (Table 7). The CC bond contracts by 66%, and the NC bond conracts by 40% of the magnitude that the CN bond expands. The CO bond shows the least displacement, with an expansion 29% of that of the CN bond. For NMA we calculate a significantly higher amide II intensity relative to amide III. In contrast, for $^{13}CH_3CNHCH_3$ in water the amide II and III relative intensities fit within 10% (Figure 6). The calculation finds, however, too small an amide I contribution.

Table 8. Calculated Raman Cross Sections of NMA, NMAD, CD_3-NMA and CD_3-NMAD

modes (cm^{-1})	relative Raman cross sections	calculated[a] Raman cross sections mbarn/mol·str
	NMA	
638	0.033	39
879	0.001	0.06
1306	0.124	148
1382	0.036	43.7
1421	0.001	0.04
1444	0.015	18
1468	0.004	5
1585	0.320	382
1623	0.017	20
	NMAD	
635	0.029	35
867	0.002	0.4
998	0.004	5
1374	0.000	0.00
1415	0.029	34
1431	0.008	10
1517	1.000	1190
1615	0.023	28
	CD_3-NMA	
592	0.026	31
866	0.001	0.4
1121	0.002	2.0
1332	0.191	227
1421	0.001	0.1
1444	0.000	0.00
1467	0.007	3.00
1582	0.314	373
1615	0.045	53
	CD_3-NMAD	
589	0.023	27
854	0.005	2.0
966	0.011	14
1050	0.004	0.4
1416	0.022	27
1443	0.000	0.00
1467	0.008	3
1510	1.103	1310
1606	0.016	19

[a] The absolute values are scaled to the experimental value of the amide II′ band of NMAD.

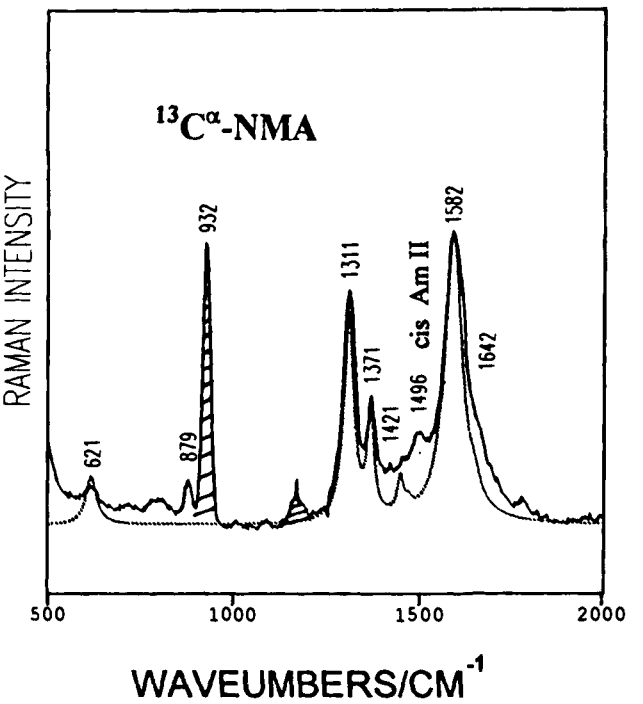

Figure 6. Comparison of the measured and calculated 218 nm excited spectrum of trans $^{13}CH_3CONHCH_3$ in water (42 mM). Bandwidths are as in Figure 5. See text for details.

Table 9. Calculated Excited State Displacements of NMAD for the Amide II′ Mode for $|\Delta| = 2.5$ and $\Gamma = 1400$ cm^{-1}

modes			Δ
1626 cm^{-1} (amide I′)			0
1514/1493 cm^{-1} (amide II′)			+2.5
1411 cm^{-1}			0
873 cm^{-1}			0
632 cm^{-1} (amide IV′)			0
Displacements in Internal Coordinates (Å)			
ΔCN	0.15	ΔND	0.01
ΔCO	0.06	$\Delta C^{\alpha}H$	0.003
ΔCC	−0.13	$\Delta C^{\beta}H$	0.001
ΔNC	−0.08		

The calculation above estimates *relative* bond length changes; additional information is required to calculate absolute bond length changes. Unfortunately, we are unable to extract the absolute values of Δ_i from either an excitation profile study or from an examination of the overtone enhancement patterns. However, we can use the results of Hudson et al.'s NMA absorption spectral modeling,[2b] which found that $\Delta = 2.5$ and $\Gamma = 1400$ cm^{-1} for the amide II′ band of NMAD. We utilize these values and eqs 1 and 2 to calculate the absolute bond length and bond angle changes in the $\pi\pi^*$ state of NMAD (Table 9). The calculation assumes that the molecule remains planar. The CN and CO bond lengths are calculated to expand by 0.15 and 0.06 Å, while the CC and NC bond lengths contract by 0.13 and 0.08 Å. Only a small 0.01 Å expansion is calculated for the NH bond length. The changes in the CN and CC bond lengths are similar to those expected between single and double bonds; this calculation suggests that in the $\pi\pi^*$ excited state the CN bonding dramatically decreases while the CC linkage gains double bond character. The double bond character of the carbonyl also decreases, while that of the NC increases. It is well known that the CN bond in the ground state is rather short due to its partial double bond character.

IV. Environmental Dependence of Excited State Geometry. The resonance Raman spectra of the NMA isotopomers dramatically change from water (Figure 2A, left) to dry non-hydrogen-bonding solvents like acetonitrile (Figure 7), and for neat NMA and for NMA in the gas phase,[2e] the amide I intensities increase while the intensities of the amide II band and the CCH_3 sb band decrease. Mayne and Hudson[2a,be] earlier considered this problem and suggested that the origin of these changes might be alterations in the normal mode composition, since their absorption spectral measurements indicated essentially identical absorption spectra for NMA in acetonitrile and water. This suggested that the electronic states were similar and required the difference to result from changes in the normal mode composition. However, Wang et al.[3b] recently reported that the NMA molar absorptivities differ by a factor of 2 between water and dry CH_3CN. We have repeated the absorption measurements and agree with Hudson et al. that little change occurs.

More recently Hudson[2d] used *ab initio* methods to calculate the contrained in-plane geometry of NMA in the $\pi\pi^*$ excited state. From these calculations they find that the $\pi\pi^*$ excited state geometry differs between isolated, dry NMA and NMA with hyrogen-bonded water molecules; the major excited state distortion occurs along the CN bond for NMA with hydrogen-bonded water. Instead, for dry NMA, Hudson finds that the

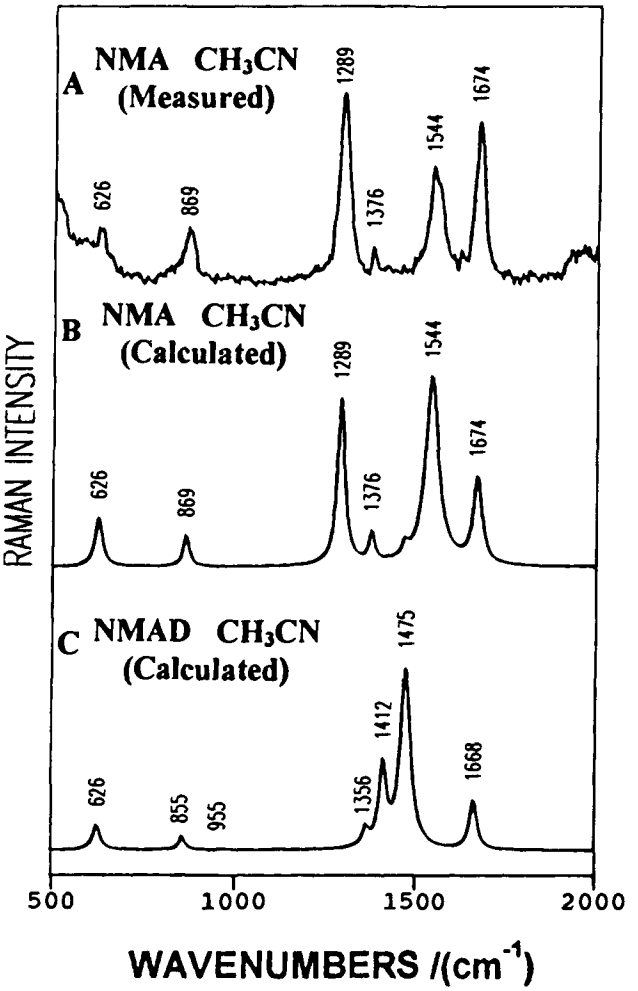

Figure 7. Measured and calculated UV resonance Raman spectra (λ = 200 mm) of trans NMA and NMAD in dry acetonirile. (A) Experimentally measured spectra of ca. 5 mM NMA. (B) Calculated NMA spectra utilizing displacements from aqueous NMA, but utilizing isolated NMA normal mode internal coordinate eigenvectors. (C) Calculated NMAD spectra utilizing the aqueous NMA displacements, but utilizing the isolated NMAD normal mode internal coordinate eigenvectors. Bandwidths are as in Figure 5.

largest distortion occurs along the CO bond. Thus, they explain the differences in the resonance Raman enhancements as deriving from excited state geometry differences.

If the excited state remains the same between solvents, we should be able to model the changes in the Raman intensity of the NMA isotopomers water and dry NMA by recalculating the spectra using the normal mode composition of isolated NMA versus NMA hydrogen bonded to water. If we are unsuccessful, then we will have to modify the excited state displacements in order to obtain good fits.

The observed resonance Raman relative intensity ratios for NMA in water for amide I, II, and III and the CCH_3 sb at 1380 cm^{-1} are 0.25:1:1:0.25. In contrast, for NMA in dry acetonitrile the observed integrated intensity ratio becomes 1:1:1:0.1. If we use the normal mode composition for NMA without water and the best-fit excited state displacements of column 1 in Table 7, we predict relative intensity ratios of 0.33:1:0.6:0.1 (Figure 7b), which approaches the observed ratios, but the amide I relative intensity is still too low. We can model a spectrum almost identical to that of NMA in acetonitrile by increasing the CO expansion by 50%, while decreasing the CC and NC contractions by ca. 20% (Figure 8A and Table 7). The intensity of the amide II band appears somewhat too large.

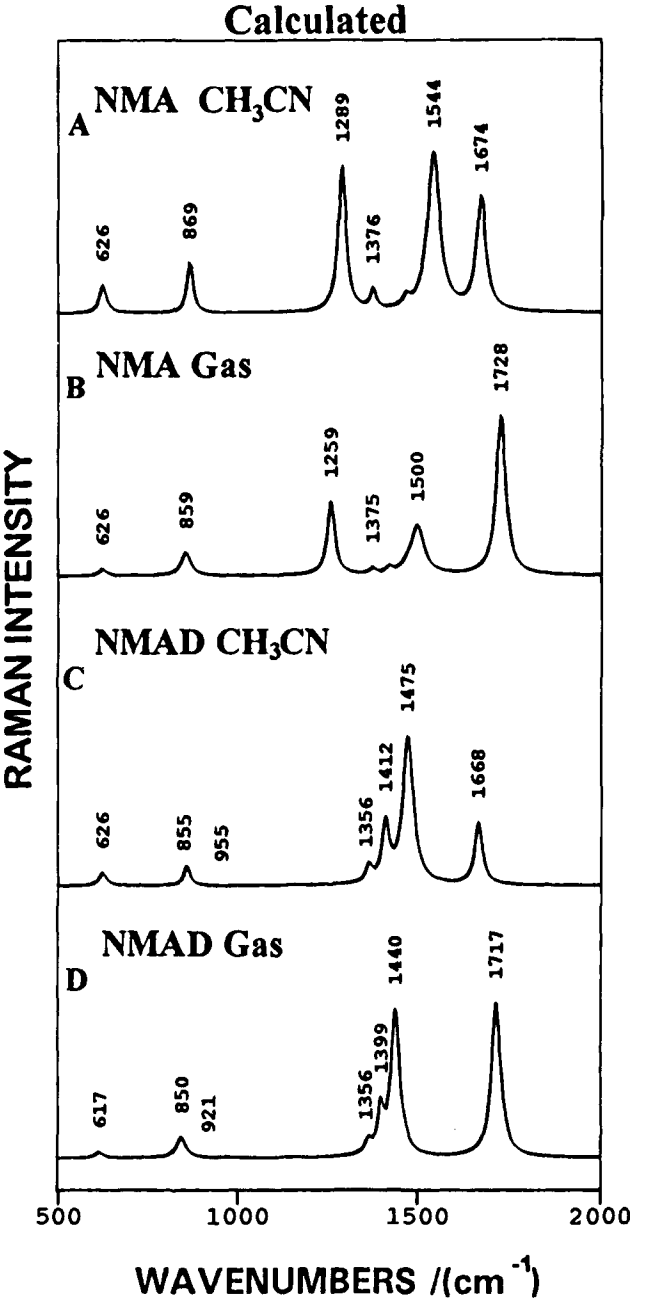

Figure 8. Calculated resonance Raman spectra of trans NMA and NMAD in dry acetonitrile and in the gas phase. The calculation utilizes the internal coordinate normal mode eignvectors of isolated NMA and NMAD and the optimized displacements. See text for details. Bandwidths are as in Figure 5.

The calculated NMAD spectrum in acetonitrile (Figure 8C) closely fits the observed spectra of Hudson and Mayne,[2e] where we predict not only the amide I′/II′ relative intensity but also the intensity of the NCH_3 sb band at 1412 cm^{-1} (see Figure 1b of ref 2e). Calculations of the gas phase NMA and NMAD spectra (Figure 8B and D) require much larger changes in the excited state displacements; the magnitude of the expansion of the CO bond approaches that of the CN bond (Table 7). This increased CO displacement permits us to calculate gas phase spectra which are indeed dominated by the amide I and I′ bands. Our calculated gas phase NMA spectra are very close to that displayed in Figure 5 of Mayne and Hudson.[2e] We correctly calculate the amide I′/II′ relative intensity for gas phase NMAD, but our calculated intensity of the 1399 cm^{-1} NCH_3 sb is less than 50% of that observed.

It appears that a major part of the spectral differences between aqueous NMA and NMA in acetonitrile results from the changes in the normal coordinates. Additional changes also occur between the displacements of the ground and excited states of NMA in water compared to NMA in acetonitrile and neat NMA and gas phase NMA. This result may support Hudson's calculations, which indicate a large dependence of the NMA $\pi\pi^*$ excited state geometry on the solvent environment. However, the increased carbonyl bond length of ground state aqueous NMA which occurs due to water hydrogen bonding would decrease the net CO displacement compared to that of the non-hydrogen-bonded cases. Separating these effects requires determination of the ground state and excited state CO bond lengths for each NMA species.

Conclusions

We have examined the near-IR, visible, and UV Raman spectra of NMA isotopomers and have characterized their Raman excitation profiles. We have calcualted the excited state bond displacements and are able to model the observed spectra of all of the isotopomers in water. Our results indicate that the alterations in the resonance Raman enhancement for NMA in non-hydrogen-bonding solvents involves both normal mode composition changes and excited state geometry changes. The CO bond of NMA is more elongated in the $\pi\pi^*$ excited state of the non-hydrogen-bonded solvents. The further change for gas phase NMA results from an even larger expansion along the CO bond. Our results also explain the surprising enhancement of the C-methyl symmetric hydrogen bending vibration by the amide $\pi \rightarrow \pi^*$ transition. The enhancement of this vibration for NMA results from a minor C−C stretching contribution. No enhancement of the analogous vibration occurs in NMAD because this vibration is almost pure C−H bending motion. The C−CD_3 symmetric bending vibrations of CD_3-NMA and CD_3-NMAD are not enhanced even though these vibrations have contributions from other motions. This lack of enhancement results from the fortuitous cancellation of Franck−Condon activities of these internal motions. Obviously, the degree of enhancement shown by the C-methyl symmetric hydrogen bending vibration is extremely sensitive to the details of the normal mode composition.

These results are relevant to understanding the secondary structure dependence of the UV Raman spectra of peptides and proteins. The spectral changes are likely to result from both changes in the normal mode composition and from changes in the excited state geometries. Thus, the understanding and the incisive use of resonance Raman spectroscopy for secondary structure investigations will require accurate normal mode calculations of the different secondary structures.

Acknowledgment. We dedicate this paper to the late Dr. Sunho Song who began the work which we report here. We gratefully acknowledge support from NIH grant R01GM30741-12 to S.A.A. and NSF grants MCB-9115906 and DMR-9110353 to S.K. R.S.S. acknowledges fellowship support from the Max Kade foundation.

JA9426150